

## Experimental study of $\eta_c$ decays into vector-vector final states

M. Ablikim<sup>1</sup>, J. Z. Bai<sup>1</sup>, Y. Ban<sup>11</sup>, J. G. Bian<sup>1</sup>, X. Cai<sup>1</sup>, H. F. Chen<sup>16</sup>, H. S. Chen<sup>1</sup>, H. X. Chen<sup>1</sup>, J. C. Chen<sup>1</sup>, Jin Chen<sup>1</sup>, Y. B. Chen<sup>1</sup>, S. P. Chi<sup>2</sup>, Y. P. Chu<sup>1</sup>, X. Z. Cui<sup>1</sup>, Y. S. Dai<sup>18</sup>, Z. Y. Deng<sup>1</sup>, L. Y. Dong<sup>1a</sup>, Q. F. Dong<sup>14</sup>, S. X. Du<sup>1</sup>, Z. Z. Du<sup>1</sup>, J. Fang<sup>1</sup>, S. S. Fang<sup>2</sup>, C. D. Fu<sup>1</sup>, C. S. Gao<sup>1</sup>, Y. N. Gao<sup>14</sup>, S. D. Gu<sup>1</sup>, Y. T. Gu<sup>4</sup>, Y. N. Guo<sup>1</sup>, Y. Q. Guo<sup>1</sup>, Z. J. Guo<sup>15</sup>, F. A. Harris<sup>15</sup>, K. L. He<sup>1</sup>, M. He<sup>12</sup>, Y. K. Heng<sup>1</sup>, H. M. Hu<sup>1</sup>, T. Hu<sup>1</sup>, G. S. Huang<sup>1b</sup>, X. P. Huang<sup>1</sup>, X. T. Huang<sup>12</sup>, X. B. Ji<sup>1</sup>, X. S. Jiang<sup>1</sup>, J. B. Jiao<sup>12</sup>, D. P. Jin<sup>1</sup>, S. Jin<sup>1</sup>, Yi Jin<sup>1</sup>, Y. F. Lai<sup>1</sup>, G. Li<sup>2</sup>, H. B. Li<sup>1</sup>, H. H. Li<sup>1</sup>, J. Li<sup>1</sup>, R. Y. Li<sup>1</sup>, S. M. Li<sup>1</sup>, W. D. Li<sup>1</sup>, W. G. Li<sup>1</sup>, X. L. Li<sup>8</sup>, X. Q. Li<sup>10</sup>, Y. L. Li<sup>4</sup>, Y. F. Liang<sup>13</sup>, H. B. Liao<sup>6</sup>, C. X. Liu<sup>1</sup>, F. Liu<sup>6</sup>, Fang Liu<sup>16</sup>, H. H. Liu<sup>1</sup>, H. M. Liu<sup>1</sup>, J. Liu<sup>11</sup>, J. B. Liu<sup>1</sup>, J. P. Liu<sup>17</sup>, R. G. Liu<sup>1</sup>, Z. A. Liu<sup>1</sup>, F. Lu<sup>1</sup>, G. R. Lu<sup>5</sup>, H. J. Lu<sup>16</sup>, J. G. Lu<sup>1</sup>, C. L. Luo<sup>9</sup>, F. C. Ma<sup>8</sup>, H. L. Ma<sup>1</sup>, L. L. Ma<sup>1</sup>, Q. M. Ma<sup>1</sup>, X. B. Ma<sup>5</sup>, Z. P. Mao<sup>1</sup>, X. H. Mo<sup>1</sup>, J. Nie<sup>1</sup>, S. L. Olsen<sup>15</sup>, H. P. Peng<sup>16</sup>, N. D. Qi<sup>1</sup>, H. Qin<sup>9</sup>, J. F. Qiu<sup>1</sup>, Z. Y. Ren<sup>1</sup>, G. Rong<sup>1</sup>, L. Y. Shan<sup>1</sup>, L. Shang<sup>1</sup>, D. L. Shen<sup>1</sup>, X. Y. Shen<sup>1</sup>, H. Y. Sheng<sup>1</sup>, F. Shi<sup>1</sup>, X. Shi<sup>1c</sup>, H. S. Sun<sup>1</sup>, J. F. Sun<sup>1</sup>, S. S. Sun<sup>1</sup>, Y. Z. Sun<sup>1</sup>, Z. J. Sun<sup>1</sup>, Z. Q. Tan<sup>4</sup>, X. Tang<sup>1</sup>, Y. R. Tian<sup>14</sup>, G. L. Tong<sup>1</sup>, G. S. Varner<sup>15</sup>, D. Y. Wang<sup>1</sup>, L. Wang<sup>1</sup>, L. S. Wang<sup>1</sup>, M. Wang<sup>1</sup>, P. Wang<sup>1</sup>, P. L. Wang<sup>1</sup>, W. F. Wang<sup>1d</sup>, Y. F. Wang<sup>1</sup>, Z. Wang<sup>1</sup>, Z. Y. Wang<sup>1</sup>, Zhe Wang<sup>1</sup>, Zheng Wang<sup>2</sup>, C. L. Wei<sup>1</sup>, D. H. Wei<sup>1</sup>, N. Wu<sup>1</sup>, X. M. Xia<sup>1</sup>, X. X. Xie<sup>1</sup>, B. Xin<sup>8b</sup>, G. F. Xu<sup>1</sup>, Y. Xu<sup>10</sup>, M. L. Yan<sup>16</sup>, F. Yang<sup>10</sup>, H. X. Yang<sup>1</sup>, J. Yang<sup>16</sup>, Y. X. Yang<sup>3</sup>, M. H. Ye<sup>2</sup>, Y. X. Ye<sup>16</sup>, Z. Y. Yi<sup>1</sup>, G. W. Yu<sup>1</sup>, C. Z. Yuan<sup>1</sup>, J. M. Yuan<sup>1</sup>, Y. Yuan<sup>1</sup>, S. L. Zang<sup>1</sup>, Y. Zeng<sup>7</sup>, Yu Zeng<sup>1</sup>, B. X. Zhang<sup>1</sup>, B. Y. Zhang<sup>1</sup>, C. C. Zhang<sup>1</sup>, D. H. Zhang<sup>1</sup>, H. Y. Zhang<sup>1</sup>, J. W. Zhang<sup>1</sup>, J. Y. Zhang<sup>1</sup>, Q. J. Zhang<sup>1</sup>, X. M. Zhang<sup>1</sup>, X. Y. Zhang<sup>12</sup>, Yiyun Zhang<sup>13</sup>, Z. P. Zhang<sup>16</sup>, Z. Q. Zhang<sup>5</sup>, D. X. Zhao<sup>1</sup>, J. W. Zhao<sup>1</sup>, M. G. Zhao<sup>10</sup>, P. P. Zhao<sup>1</sup>, W. R. Zhao<sup>1</sup>, Z. G. Zhao<sup>1e</sup>, H. Q. Zheng<sup>11</sup>, J. P. Zheng<sup>1</sup>, Z. P. Zheng<sup>1</sup>, L. Zhou<sup>1</sup>, N. F. Zhou<sup>1</sup>, K. J. Zhu<sup>1</sup>, Q. M. Zhu<sup>1</sup>, Y. C. Zhu<sup>1</sup>, Y. S. Zhu<sup>1</sup>, Yingchun Zhu<sup>1f</sup>, Z. A. Zhu<sup>1</sup>, B. A. Zhuang<sup>1</sup>, X. A. Zhuang<sup>1</sup>, B. S. Zou<sup>1</sup>

(BES Collaboration)

<sup>1</sup> Institute of High Energy Physics, Beijing 100049, People's Republic of China

<sup>2</sup> China Center for Advanced Science and Technology (CCAST), Beijing 100080, People's Republic of China

<sup>3</sup> Guangxi Normal University, Guilin 541004, People's Republic of China

<sup>4</sup> Guangxi University, Nanning 530004, People's Republic of China

<sup>5</sup> Henan Normal University, Xinxiang 453002, People's Republic of China

<sup>6</sup> Huazhong Normal University, Wuhan 430079, People's Republic of China

<sup>7</sup> Hunan University, Changsha 410082, People's Republic of China

<sup>8</sup> Liaoning University, Shenyang 110036, People's Republic of China

<sup>9</sup> Nanjing Normal University, Nanjing 210097, People's Republic of China

<sup>10</sup> Nankai University, Tianjin 300071, People's Republic of China

<sup>11</sup> Peking University, Beijing 100871, People's Republic of China

<sup>12</sup> Shandong University, Jinan 250100, People's Republic of China

<sup>13</sup> Sichuan University, Chengdu 610064, People's Republic of China

<sup>14</sup> Tsinghua University, Beijing 100084, People's Republic of China

<sup>15</sup> University of Hawaii, Honolulu, HI 96822, USA

<sup>16</sup> University of Science and Technology of China, Hefei 230026, People's Republic of China

<sup>17</sup> Wuhan University, Wuhan 430072, People's Republic of China

<sup>18</sup> Zhejiang University, Hangzhou 310028, People's Republic of China

<sup>a</sup> Current address: Iowa State University, Ames, IA 50011-3160, USA

<sup>b</sup> Current address: Purdue University, West Lafayette, IN 47907, USA

<sup>c</sup> Current address: Cornell University, Ithaca, NY 14853, USA

<sup>d</sup> Current address: Laboratoire de l'Accélérateur Linéaire, Orsay, F-91898, France

<sup>e</sup> Current address: University of Michigan, Ann Arbor, MI 48109, USA

<sup>f</sup> Current address: DESY, D-22607, Hamburg, Germany

Using 58 million  $J/\psi$  events accumulated with the BESII detector, branching fractions for the  $\eta_c \rightarrow VV$  decays,  $\eta_c \rightarrow \rho\rho$ ,  $\eta_c \rightarrow K^*\bar{K}^*$ ,  $\eta_c \rightarrow \omega\omega$ , and  $\eta_c \rightarrow \phi\phi$ , are measured. The branching fractions are  $Br(\eta_c \rightarrow \rho\rho) = (1.25 \pm 0.37 \pm 0.51) \times 10^{-2}$ ,  $Br(\eta_c \rightarrow K^*\bar{K}^*) = (10.4 \pm 2.6 \pm 4.3) \times 10^{-3}$ ,  $Br(\eta_c \rightarrow \omega\omega) < 6.3 \times 10^{-3}$  (90 % CL), and  $Br(\eta_c \rightarrow \phi\phi) = (2.5 \pm 0.5 \pm 0.9) \times 10^{-3}$ . The process  $\eta_c \rightarrow \omega\phi$  is also searched for, and the 90% CL upper limit  $Br(\eta_c \rightarrow \omega\phi) < 1.3 \times 10^{-3}$  is obtained for this process.

## I. INTRODUCTION

It has been known for many years that  $\eta_c$  decays into vector-vector (VV) mesons, even though this process is forbidden by hadron helicity conservation (HHC) assuming collinear valence quark configurations dominate. Three different Bethe-Salpeter wave functions (Gauss, Exponent, Power) have been used to calculate  $\text{Br}(\eta_c \rightarrow VV)$  [2]; the calculated results are lower than the experimental ones from the PDG [1] by two or three orders of magnitude, as shown in Table I. New theoretical predictions are needed.

TABLE I: Theoretical predictions for  $\text{Br}(\eta_c \rightarrow VV)$  compared with PDG results [1]. Gauss, Exponent, and Power refer to three different Bethe-Salpeter wave functions used to calculate  $\text{Br}(\eta_c \rightarrow VV)$  [2].

Br	Gauss	Exponent	Power	PDG
$\text{Br}(\eta_c \rightarrow \rho\rho)$	$2.3 \times 10^{-5}$	$8.7 \times 10^{-5}$	$2.8 \times 10^{-4}$	$(2.6 \pm 0.9) \times 10^{-2}$
$\text{Br}(\eta_c \rightarrow K^*\bar{K}^*)$	$2.8 \times 10^{-5}$	$8.6 \times 10^{-5}$	$2.8 \times 10^{-4}$	$(8.5 \pm 3.1) \times 10^{-3}$
$\text{Br}(\eta_c \rightarrow \phi\phi)$	$4.2 \times 10^{-6}$	$1.6 \times 10^{-5}$	$5.0 \times 10^{-5}$	$(2.6 \pm 0.9) \times 10^{-3}$

Branching fractions and reduced branching fractions,  $BR_R$ , compared with SU(3) predictions [4] are shown in Table II. Here the reduced branching fraction is defined as  $BR_R = BR/(P_V^3)$ , where  $P_V$  is the momentum of the vector meson in the  $\eta_c$  center-of-mass system. The experimental results are not inconsistent with SU(3) expectations, but due to the large errors no meaningful investigation of possible SU(3) symmetry breaking patterns can be performed.

TABLE II: Comparison of PDG  $\text{Br}(\eta_c \rightarrow VV)$  results with predictions of SU(3) symmetry. Ratio of  $BR_R$  is defined as  $BR_R(\eta_c \rightarrow VV)/BR_R(\eta_c \rightarrow \phi\phi)$ , and this can be compared with the SU(3) expectation, SU(3).

	BR( $10^{-3}$ )	$BR_R(10^{-3})$	Ratio of $BR_R$	SU(3)
$\text{Br}(\eta_c \rightarrow \rho\rho)$	$26 \pm 9$	$12.6 \pm 4.4$	$6.3 \pm 2.3$	3
$\text{Br}(\eta_c \rightarrow K^*\bar{K}^*)$	$8.5 \pm 3.1$	$5 \pm 1.7$	$2.5 \pm 0.9$	4
$\text{Br}(\eta_c \rightarrow \omega\omega)$	$< 3.1$	$< 1.5$	$< 0.8$	1
$\text{Br}(\eta_c \rightarrow \phi\phi)$	$2.6 \pm 0.9$	$2 \pm 0.7$	$1 \pm 0.4$	1

Exclusive decays of  $\eta_c$  into vector meson pairs have also been investigated in the framework of the  $^3P_0$  quark-creation model [3]. The width of  $\eta_c \rightarrow \rho^0\rho^0$  in PDG is significantly larger than the model prediction. The branching fraction of  $\eta_c \rightarrow \omega\phi$  is very important to determine the mechanism of  $\eta_c \rightarrow VV$  decay [5]. In this paper,  $J/\psi \rightarrow \gamma\eta_c$  decays from a sample of 58 million  $J/\psi$  decays obtained with the BESII detector are used to determine  $\text{Br}(\eta_c \rightarrow \rho\rho)$ ,  $\text{Br}(\eta_c \rightarrow K^*\bar{K}^*)$ ,  $\text{Br}(\eta_c \rightarrow \omega\omega)$ ,  $\text{Br}(\eta_c \rightarrow \phi\phi)$ , and  $\text{Br}(\eta_c \rightarrow \omega\phi)$ .

## II. BES DETECTOR

BES is a conventional solenoidal magnet detector [6, 7]. A 12-layer vertex chamber (VTC) surrounding the beam pipe provides trigger and trajectory information. A forty-layer main drift chamber (MDC), located radially outside the VTC, provides trajectory and energy loss ( $dE/dx$ ) information for charged tracks over 85% of the total solid angle with a momentum resolution of  $\sigma_p/p = 0.0178\sqrt{1+p^2}$  ( $p$  in GeV/ $c$ ) and a  $dE/dx$  resolution for hadron tracks of  $\sim 8\%$ . An array of 48 scintillation counters surrounding the MDC measures the time-of-flight (TOF) of charged tracks with a resolution of  $\sim 200$  ps for hadrons. Radially outside the TOF system is a 12 radiation length, lead-gas barrel shower counter (BSC). This measures the energies of electrons and photons over  $\sim 80\%$  of the total solid angle with an energy resolution of  $\sigma_E/E = 21\%/\sqrt{E}$  ( $E$  in GeV). Outside the solenoidal coil, which provides a 0.4 Tesla magnetic field over the tracking volume, is an iron flux return that is instrumented with three double layers of proportional counters that identify muons of momentum greater than 0.5 GeV/ $c$ .

A Geant3 based Monte Carlo, SIMBES [8], which simulates the detector response, including interactions of secondary particles in the detector material, is used in this analysis. Reasonable agreement between data and Monte Carlo simulation is observed in various channels tested, including  $e^+e^- \rightarrow (\gamma)e^+e^-$ ,  $e^+e^- \rightarrow (\gamma)\mu\mu$ ,  $J/\psi \rightarrow p\bar{p}$ ,  $J/\psi \rightarrow \rho\pi$ , and  $\psi(2S) \rightarrow \pi^+\pi^-J/\psi$ ,  $J/\psi \rightarrow l^+l^-$ . For  $J/\psi \rightarrow \gamma\eta_c$ , decays are generated with an angular distribution of  $1 + \cos^2\theta$ , where  $\theta$  is the angle between the  $e^+$  and  $\eta_c$  in the laboratory.

### III. $\eta_c \rightarrow \rho^0 \rho^0$

#### A. Event selection

First a  $J/\psi \rightarrow \gamma\pi^+\pi^-\pi^+\pi^-$  sample is selected. Events are required to have four good charged tracks and one or more photon candidates. A good track, reconstructed from hits in the MDC, must be well fitted to a helix originating from the interaction point; have a polar angle,  $\theta$ , with  $|\cos\theta| < 0.8$ ; and a transverse momentum greater than 60 MeV/c. TOF and  $dE/dx$  information are combined to form particle identification probabilities for the pion, kaon, and proton hypotheses. At least three tracks must be identified as pions. To reduce the number of spurious low energy photons produced by secondary hadronic interactions, photon candidates must have a minimum energy of 50 MeV and be outside a cone with a half-angle of  $15^\circ$  around any charged track.

To get improved momentum resolution and to remove backgrounds, events are kinematically fitted to the  $J/\psi \rightarrow \gamma\pi^+\pi^-\pi^+\pi^-$  hypothesis, using all photon candidates. The fit with the highest probability is selected, and the  $\chi^2$  of the four constraint (4C) fit is required to be less than 20.

For  $J/\psi \rightarrow \gamma\pi^+\pi^-\pi^+\pi^-$  decay, a major source of background is from  $J/\psi \rightarrow \pi^0\pi^+\pi^-\pi^+\pi^-$ . To remove events containing a  $\pi^0$ , when there are multiple photons,  $|m_{\gamma_1\gamma_2} - m_{\pi^0}| > 60$  MeV/c<sup>2</sup> is required if  $\vec{P}_{miss}$  is near the plane of the two photons,  $\gamma_1$  and  $\gamma_2$ , i.e.  $|\hat{P}_{miss} \cdot (\hat{r}_{\gamma_1} \times \hat{r}_{\gamma_2})| < 0.15$ . Here  $\hat{P}_{miss}$  is the unit vector of the missing momentum of all charged tracks;  $\hat{r}_{\gamma_1}$  and  $\hat{r}_{\gamma_2}$  are unit vectors in the  $\gamma_1$  and  $\gamma_2$  directions, respectively; and  $m_{\gamma_1\gamma_2}$  is the invariant mass of  $\gamma_1$  and  $\gamma_2$ . Two additional requirements,  $\chi^2(J/\psi \rightarrow \gamma\pi^+\pi^-\pi^+\pi^-) < \chi^2(J/\psi \rightarrow \gamma\gamma\pi^+\pi^-\pi^+\pi^-)$  and  $P_{t\gamma}^2 < 0.0015$  (GeV/c)<sup>2</sup>, are used to further remove  $J/\psi \rightarrow \pi^0\pi^+\pi^-\pi^+\pi^-$  background.  $P_{t\gamma}$  is the transverse momentum of the  $\pi^+\pi^-\pi^+\pi^-$  system with respect to the photon. Finally, the requirement  $|U_{miss}| = |E_{miss} - cP_{miss}| < 0.07$  GeV/c is used to reject events with multiple photons or charged kaons; here,  $E_{miss}$  and  $P_{miss}$  are, respectively, the missing energy and missing momentum calculated using only the charged particles, which are assumed to be pions.

There are other possible backgrounds such as  $J/\psi \rightarrow \omega\pi^+\pi^-$ ,  $J/\psi \rightarrow \gamma K_s^0 K_s^0$ , and  $J/\psi \rightarrow \gamma K_s^0 K^\pm \pi^\mp$ . The  $J/\psi \rightarrow \omega\pi^+\pi^-$  background is suppressed by the requirement  $|M_{\pi^+\pi^-\pi^0} - M_\omega| > 40$  MeV/c<sup>2</sup>, where the  $\pi^0$  in  $\pi^0\pi^+\pi^-\pi^+\pi^-$  is associated to the missing momentum and energy, determined using only the charged tracks. To remove the  $J/\psi \rightarrow \gamma K_s^0 K_s^0$  background,  $|M_{\pi^+\pi^-} - M_{K_s^0}| > 25$  MeV/c<sup>2</sup> is required for both  $\pi^+\pi^-$  pairs. To remove the background from  $J/\psi \rightarrow \gamma K_s^0 K^\pm \pi^\mp$ , events are rejected if  $\chi^2(J/\psi \rightarrow \gamma K^\pm \pi^\mp \pi^+ \pi^-) < \chi^2(J/\psi \rightarrow \gamma \pi^+ \pi^- \pi^+ \pi^-)$  when  $|M_{\pi^+\pi^-} - M_{K_s^0}| < 25$  MeV/c<sup>2</sup>.

Figure 1 shows the scatter plot of  $M_{\pi_2\pi_3}$  versus  $M_{\pi_1\pi_4}$  for surviving events with  $M_{\pi^+\pi^-\pi^+\pi^-} \geq 2.8$  GeV/c<sup>2</sup>, where  $\pi_1$  ( $\pi_3$ ) and  $\pi_2$  ( $\pi_4$ ) are the  $\pi^+$  and  $\pi^-$  with the higher (lower) momentum. There are clear signals near  $(M_{\rho^0}, M_{\rho^0})$  and  $(M_{f_2(1270)}, M_{f_2(1270)})$ . The decay  $J/\psi \rightarrow \gamma f_2 f_2$ , including  $\eta_c \rightarrow f_2 f_2$ , has been studied previously using the  $J/\psi$  events collected by BES II [9].

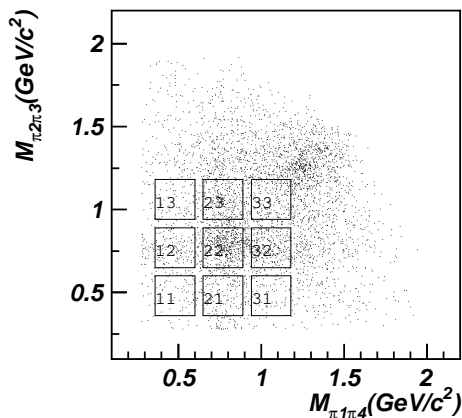


FIG. 1: Scatterplot of  $M_{\pi_2\pi_3}$  versus  $M_{\pi_1\pi_4}$ . Also shown are the signal and sideband background boxes used in this analysis.

The number of  $\eta_c \rightarrow \rho^0 \rho^0$  events and the corresponding backgrounds are estimated from the boxes in the scatter plot of  $\pi^+\pi^-$  versus  $\pi^+\pi^-$  invariant masses, as shown in Fig. 1. The signal region is shown as the square box 22 at  $(0.77, 0.77)$  GeV/c<sup>2</sup> with a width of 240 MeV/c<sup>2</sup>. The main backgrounds are  $\eta_c \rightarrow \rho\pi^+\pi^-$  and  $\eta_c \rightarrow \pi^+\pi^-\pi^+\pi^-$ . The  $\eta_c \rightarrow \rho\pi^+\pi^-$  background produces the horizontal and vertical bands at  $m_\rho$ , and the  $\eta_c \rightarrow \pi^+\pi^-\pi^+\pi^-$  background produces the uniform background in the  $m_{\pi^+\pi^-}$  versus  $m_{\pi^+\pi^-}$  scatter plot of Fig. 1. These backgrounds are estimated

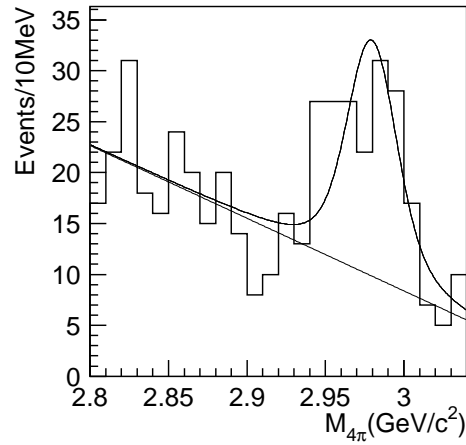


FIG. 2: Fitting  $\eta_c$  in the  $M_{\pi^+\pi^-\pi^+\pi^-}$  spectrum of events in the signal box 22 in Fig. 1. The fitted number of  $\eta_c$  events is  $N^{sig} = 106.9 \pm 18.2$ .

using the horizontal and vertical sideband background boxes, which are taken 50 MeV/c<sup>2</sup> away from the signal box and denoted as 12, 21, 32, and 23, and the two diagonal boxes, denoted as 31 and 13, in Fig. 1.

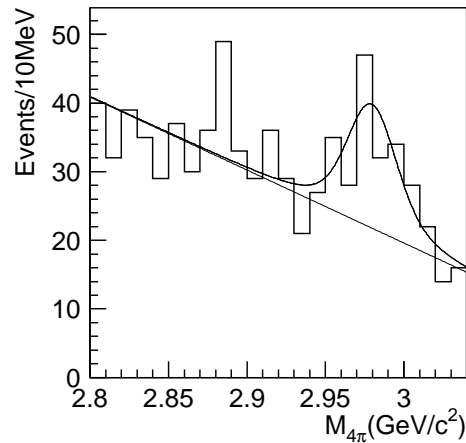


FIG. 3: Fitting  $\eta_c$  in the  $M_{\pi^+\pi^-\pi^+\pi^-}$  spectrum of four horizontal and vertical sideband boxes (12,21,32,23). The fitted number of  $\eta_c$  events is  $N^{sid1} = 83.3 \pm 21.5$ .

## B. Results

Shown in Figs. 2, 3, and 4 are the  $M_{\pi^+\pi^-\pi^+\pi^-}$  fitting results for  $\rho^0\rho^0$  signal and sideband regions. Binned maximum likelihood fits are performed with a Breit-Wigner convoluted with a Gaussian resolution function for the  $\eta_c$  and a first order polynomial for background. The number of  $\eta_c \rightarrow \rho^0\rho^0$  events is obtained with the formula  $N^{obs} = N^{sig} - N^{sid1}/2 + N^{sid2}/2$ . Here  $N^{sig}$ ,  $N^{sid1}$ , and  $N^{sid2}$  are the fitted number of  $\eta_c$  events in the  $M_{\pi^+\pi^-\pi^+\pi^-}$  signal box and sideband boxes (See Figs. 2, 3, 4). So  $N^{obs} = (106.9 \pm 18.2) - (83.3 \pm 21.5)/2 + (15.8 \pm 8.9)/2 = 73.1 \pm 21.6$ .

The  $\eta_c \rightarrow \rho^0\rho^0$  branching fraction is determined from

$$\begin{aligned} Br(\eta_c \rightarrow \rho^0\rho^0) &= \frac{N^{obs}/\epsilon}{N_{J/\psi} \cdot Br(J/\psi \rightarrow \gamma\eta_c)} \\ &= (4.15 \pm 1.23) \times 10^{-3}, \end{aligned}$$

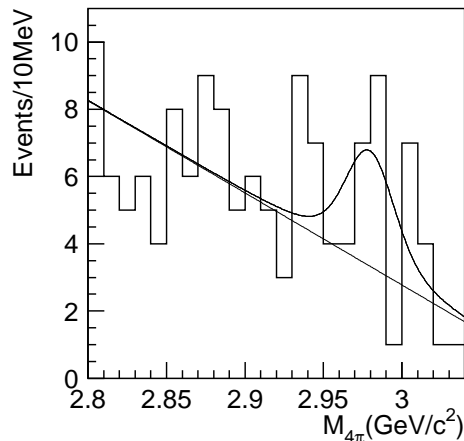


FIG. 4: Fitting  $\eta_c$  in the  $M_{\pi^+\pi^-\pi^+\pi^-}$  spectrum of two diagonal boxes (31,13). The fitted number of  $\eta_c$  events is  $N^{sid2} = 15.8 \pm 8.9$ .

where  $\varepsilon = 2.35\%$  is the efficiency, corrected for sideband subtraction, determined from Monte Carlo simulation.  $N_{J/\psi} = 57.7 \times 10^6$  is the total number of  $J/\psi$  events collected by BESII [10], and  $Br(J/\psi \rightarrow \gamma\eta_c) = 0.013$  is the branching fraction for  $J/\psi \rightarrow \gamma\eta_c$  [1]. Correcting for charged decay modes,  $Br(\eta_c \rightarrow \rho\rho) = (1.25 \pm 0.37) \times 10^{-2}$  is obtained.

#### IV. $\eta_c \rightarrow K^*\bar{K}^*$

$J/\psi \rightarrow \gamma\eta_c \rightarrow \gamma K^{*0}\bar{K}^{*0} \rightarrow \gamma\pi^+\pi^-K^+K^-$  is studied to determine the  $\eta_c \rightarrow K^*\bar{K}^*$  branching fraction.

##### A. Event Selection

The selection criteria for charged tracks and photons are the same as for the  $\eta_c \rightarrow \rho^0\rho^0$  analysis. At least one good photon is required. TOF and  $dE/dx$  information are combined to form particle identification probabilities for the pion, kaon, and proton hypotheses for each track, and at least two tracks must be identified as kaons. The same method as used in the  $\eta_c \rightarrow \rho^0\rho^0$  analysis is used to remove  $\pi^0$  background.

Some additional requirements are applied. Combined probabilities are formed from the particle identification probabilities of all tracks and the probabilities determined from the 4C kinematic fit to the  $J/\psi \rightarrow \gamma\pi^+\pi^-K^+K^-$  hypothesis for all possible combinations. The fit with the highest probability is selected, and the  $\chi^2$  of the 4C kinematic fit is required to be less than 10.

To further remove backgrounds containing  $\pi^0$ s, two requirements,  $\chi^2(J/\psi \rightarrow \gamma\pi^+\pi^-K^+K^-) < \chi^2(J/\psi \rightarrow \gamma\gamma\pi^+\pi^-K^+K^-)$  and  $P_{t\gamma}^2 < 0.003(\text{GeV}/c)^2$ , are used.  $P_{t\gamma}$  is the transverse momentum of the  $\pi^+\pi^-K^+K^-$  system with respect to the photon. Furthermore, the requirement  $|U_{miss}| = |E_{miss} - cP_{miss}| < 0.1 \text{ GeV}/c^2$  is used to reject events with multiple photons; here,  $E_{miss}$  and  $P_{miss}$  are, respectively, the missing energy and missing momentum calculated using only the charged particles, which are assumed to be  $\pi^+\pi^-K^+K^-$ .  $\chi^2(J/\psi \rightarrow \pi^+\pi^-K^+K^-) > 20$  is required to remove  $J/\psi \rightarrow \pi^+\pi^-K^+K^-$  background.

There are other possible backgrounds such as  $J/\psi \rightarrow \omega K^+K^-$ ,  $J/\psi \rightarrow \gamma K_s^0 K^\pm \pi^\mp$ , etc. The  $J/\psi \rightarrow \omega K^+K^-$  background is suppressed with the requirement  $|M_{\pi^+\pi^-\pi^0} - M_\omega| > 40 \text{ MeV}/c^2$ , where the  $\pi^0$  in  $\pi^0\pi^+\pi^-K^+K^-$  is associated to the missing momentum and energy, determined using only the charged tracks. To remove the background from  $J/\psi \rightarrow \gamma K_s^0 K^\pm \pi^\mp$ , events are rejected if  $\chi^2(J/\psi \rightarrow \gamma K^\pm \pi^\mp \pi^+ \pi^-) < \chi^2(J/\psi \rightarrow \gamma\pi^+\pi^-K^+K^-)$  when  $|M_{\pi^+\pi^-} - M_{K^0}| < 25 \text{ MeV}/c^2$ . To remove backgrounds containing  $\phi$ ,  $|M_{K^+K^-} - M_\phi| > 0.02 \text{ GeV}/c^2$  is required.

A  $K^{*0}\bar{K}^{*0}$  signal is seen in the scatter plot of  $M_{K^+\pi^-}$  versus  $M_{K^-\pi^+}$ , shown in Fig. 5. The same method is used as for the  $\eta_c \rightarrow \rho^0\rho^0$  analysis to estimate sideband background. The signal region is shown as a square box at  $(0.896, 0.896) \text{ GeV}/c^2$  with a width of  $160 \text{ MeV}/c^2$ . The main backgrounds are  $\eta_c \rightarrow K^*K\pi$  and  $\eta_c \rightarrow K^+K^-\pi^+\pi^-$ . The  $\eta_c \rightarrow K^*K\pi$  background appears as the horizontal and vertical bands at  $m_{K^*}$ , and the  $\eta_c \rightarrow K^+K^-\pi^+\pi^-$  background as the uniform background in the  $M_{K^+\pi^-}$  versus  $M_{K^-\pi^+}$  scatter plot of Fig. 5. The backgrounds

are estimated from the sideband boxes, which are taken  $40 \text{ MeV}/c^2$  away from the signal box and shown as four horizontal/vertical boxes (denoted as 12,21,32,23) and four diagonal boxes (denoted as 31,13,11,33) in Fig. 5. The horizontal and vertical sideband boxes (12,21,32,23) allow the determination of the backgrounds from the horizontal and vertical bands, while the diagonal boxes (13,31,11,33) allow the estimation of the smaller uniform background contribution. According to a Monte Carlo study, other  $\eta_c$  backgrounds such as  $\eta_c \rightarrow K^+K^-K^+K^-$  and  $\eta_c \rightarrow \pi^+\pi^-\pi^+\pi^-$  do not survive the selection criteria.

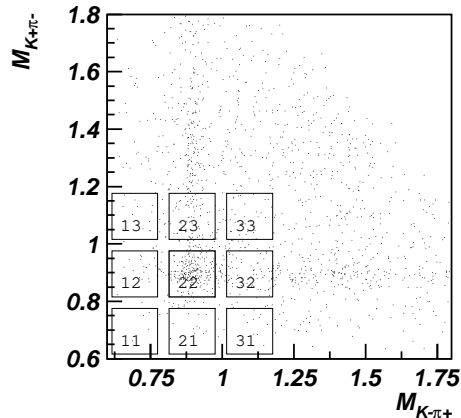


FIG. 5: Scatter plot of  $M_{K^+\pi^-}$  versus  $M_{K^-\pi^+}$ . Signal and sideband boxes used in the analysis are shown in the scatter plot.

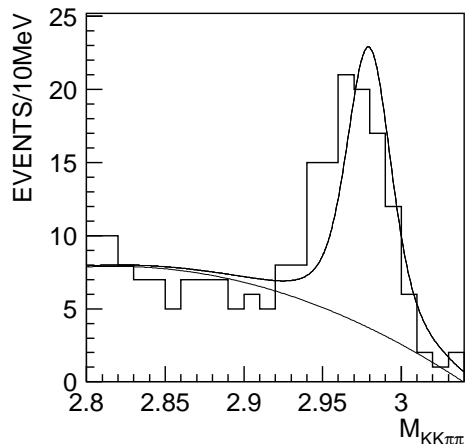


FIG. 6: Fitting  $\eta_c$  in the  $M_{\pi^+\pi^-K^+K^-}$  spectrum of events from signal box 22. The fitted number of  $\eta_c$  events is  $N^{sig} = 80.3 \pm 13.6$ .

## B. Results

Shown in Figs. 6, 7, and 8 are the  $M_{\pi^+\pi^-K^+K^-}$  fitting results for  $K^{*0}\bar{K}^{*0}$  signal and sideband regions. Binned maximum likelihood fits are performed with a Breit-Wigner convoluted with a Gaussian resolution function for the  $\eta_c$  and a second order polynomial for background. The number of  $\eta_c \rightarrow K^{*0}\bar{K}^{*0}$  events are obtained from  $N^{obs} = N^{sig} - N^{sid1}/2 + N^{sid2}/4$ . Here  $N^{sig}$ ,  $N^{sid1}$  and  $N^{sid2}$  are the fitted number of  $\eta_c$  events in the  $M_{\pi^+\pi^-K^+K^-}$  signal and sideband boxes(See Figs. 6, 7, 8). So  $N^{obs} = (80.3 \pm 13.6) - (41.0 \pm 10.2)/2 + (0.0 \pm 0.1)/4 = 59.8 \pm 14.5$ .

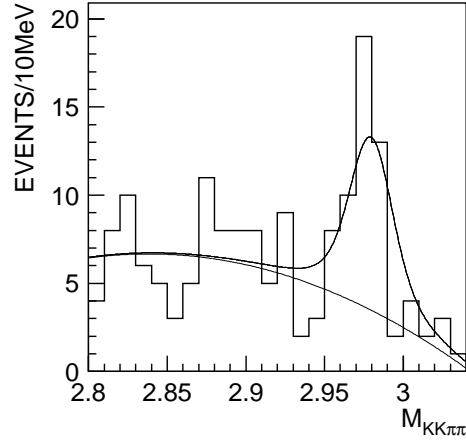


FIG. 7: Fitting  $\eta_c$  in the  $M_{\pi^+\pi^-K^+K^-}$  spectrum of events from the four horizontal and vertical sideband boxes. The fitted number of  $\eta_c$  events is  $N^{sid1} = 41.0 \pm 10.2$ .

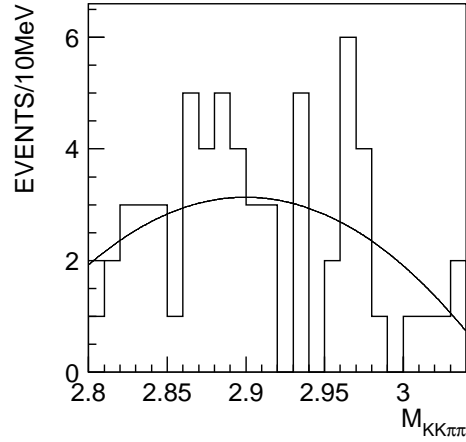


FIG. 8: Fitting  $\eta_c$  in the  $M_{\pi^+\pi^-K^+K^-}$  spectrum of events from the four diagonal boxes (31,13,11,33). The fitted number of  $\eta_c$  events is  $N^{sid2} = 0.0 \pm 0.1$ .

The branching fraction of  $\eta_c \rightarrow K^{*0}\bar{K}^{*0}$  is given by

$$\begin{aligned} Br(\eta_c \rightarrow K^{*0}\bar{K}^{*0}) &= \frac{N^{obs}/\varepsilon}{N_{J/\psi} \cdot Br(J/\psi \rightarrow \gamma\eta_c) \cdot Br^2(K^{*0}(\bar{K}^{*0}) \rightarrow K^\pm\pi^\mp)} \\ &= (5.2 \pm 1.3) \times 10^{-3}, \end{aligned}$$

where  $\varepsilon = 3.4\%$  is the efficiency, corrected for sideband subtraction, determined from Monte Carlo simulation. Using  $Br(K^{*0}(\bar{K}^{*0}) \rightarrow K^\pm\pi^\mp) = 0.67$  and correcting for charged decay modes, we obtain  $Br(\eta_c \rightarrow K^*\bar{K}^*) = (10.4 \pm 2.6) \times 10^{-3}$ .

### V. $\eta_c \rightarrow \omega\omega$

$J/\psi \rightarrow \gamma\eta_c \rightarrow \gamma\omega\omega \rightarrow \gamma\pi^0\pi^+\pi^-\pi^0\pi^+\pi^-$  is studied to obtain the branching fraction of  $\eta_c \rightarrow \omega\omega$ .

## A. Event Selection

The charged track selection criteria and particle identification are the same as in the above two analyses. Here, four tracks must be identified as pions. The photon selection criteria are different for  $\eta_c \rightarrow \omega\omega$  to get higher efficiency because there are five photons in this channel. To reduce the number of spurious low energy photons produced by secondary hadronic interactions, photon candidates must have a minimum energy of 50 MeV and be outside a cone with a half-angle of  $6^\circ$  around any charged track. At least five good photons are required.

To get improved momentum resolution and to remove backgrounds, events are kinematically fitted to the  $J/\psi \rightarrow 5\gamma\pi^+\pi^-\pi^+\pi^-$  (4C fit) and  $J/\psi \rightarrow \gamma\pi^0\pi^+\pi^-\pi^+\pi^-$  (6C fit) hypotheses, for all combinations of photon candidates.  $\chi^2_{4C}(J/\psi \rightarrow 5\gamma\pi^+\pi^-\pi^+\pi^-) < 20$  and  $\chi^2_{6C}(J/\psi \rightarrow \gamma\pi^0\pi^+\pi^-\pi^+\pi^-) < 8$  are required. To get cleaner  $J/\psi \rightarrow \gamma\omega\omega$  candidates,  $|M_{\pi^0}^1 - 0.135| < 0.035 \text{ GeV}/c^2$  and  $|M_{\pi^0}^2 - 0.135| < 0.035 \text{ GeV}/c^2$  are required. Here, the photons used for  $M_{\pi^0}^1$  and  $M_{\pi^0}^2$  are determined from the best 6C fit to the  $J/\psi \rightarrow \gamma\pi^0\pi^+\pi^-\pi^+\pi^-$  hypothesis.

## B. Results

There are four pairs of  $M_{\pi^+\pi^-\pi^0}^1$  versus  $M_{\pi^+\pi^-\pi^0}^2$  combinations for every event. If one of the combinations satisfies  $|M_{\pi^+\pi^-\pi^0}^1 - M_\omega| < 0.035 \text{ GeV}/c^2$  and  $|M_{\pi^+\pi^-\pi^0}^2 - M_\omega| < 0.035 \text{ GeV}/c^2$ , the event is selected as a  $J/\psi \rightarrow \gamma\omega\omega$  candidate. The  $M_{\pi^0\pi^+\pi^-\pi^0\pi^+\pi^-}$  distribution for  $J/\psi \rightarrow \gamma\omega\omega$  candidates is shown in Fig. 9.

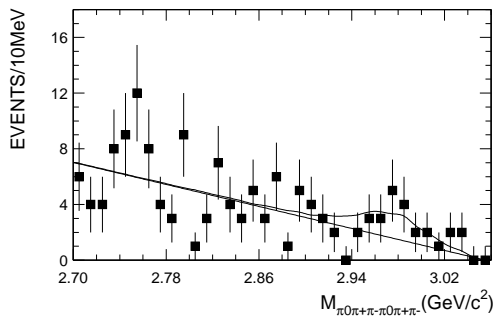


FIG. 9: The  $\eta_c$  fit of the  $M_{\pi^0\pi^+\pi^-\pi^0\pi^+\pi^-}$  distribution of candidate events in the  $\omega\omega$  region.

Figure 9 shows the result of fitting  $\eta_c$  to the  $M_{\pi^0\pi^+\pi^-\pi^0\pi^+\pi^-}$  distribution of candidate events in the  $\omega\omega$  region. The shape of the  $\eta_c$  used in the fit is obtained from Monte Carlo simulation of  $\eta_c \rightarrow \omega\omega$ . The fitted number of  $\eta_c$  events is  $16.4 \pm 9.4$ . The result has large errors and includes decays other than  $J/\psi \rightarrow \gamma\omega\omega$  decay. Therefore only the upper limit on  $Br(\eta_c \rightarrow \omega\omega)$  is determined. At the 90% confidence level, the upper limit on  $N_{\eta_c}$  is  $N_{\eta_c}^{upper} = 23$ . The upper limit on  $Br(\eta_c \rightarrow \omega\omega)$  at the 90% C.L. is determined from

$$\begin{aligned} Br(\eta_c \rightarrow \omega\omega) &< \frac{N_{\eta_c}^{upper} / \varepsilon}{N_{J/\psi} \cdot Br(J/\psi \rightarrow \gamma\eta_c) \cdot Br^2(\omega \rightarrow \pi^+\pi^-\pi^0)} \\ &= 4.0 \times 10^{-3}, \end{aligned}$$

where  $\varepsilon = 0.96\%$  is the efficiency determined from Monte Carlo and  $Br(\omega \rightarrow \pi^+\pi^-\pi^0) = 0.89$  [1].

## VI. $\eta_c \rightarrow \phi\phi$

### A. Event Selection

$J/\psi \rightarrow \gamma\phi\phi \rightarrow \gamma K^+K^-K^+K^-$  is used to study  $\eta_c \rightarrow \phi\phi$ . The branching fraction of  $\eta_c \rightarrow \phi\phi$  in the PDG is mainly determined from the BES result  $Br(\eta_c \rightarrow \phi\phi) = (2.5 \pm 0.5 \pm 0.9) \times 10^{-3}$  [13]. In order to do a systematic study of  $\eta_c \rightarrow VV$ , we also analyze the  $\eta_c \rightarrow \phi\phi$  decay, in order to remove the common systematic errors when calculating the ratios of reduced branching fractions  $BR_R(\eta_c \rightarrow VV)$ .

The selection criteria for charged tracks and particle identification are the same as those in the  $\eta_c \rightarrow \rho^0\rho^0$  analysis. At least three tracks must be identified as kaons. A 1C fit with a missing photon is performed to get better

momentum resolution. To select  $J/\psi \rightarrow \gamma\phi\phi$  candidates,  $|M_{K^+K^-} - M_\phi| < 20 \text{ MeV}/c^2$ , is required for both  $K^+K^-$  invariant masses.

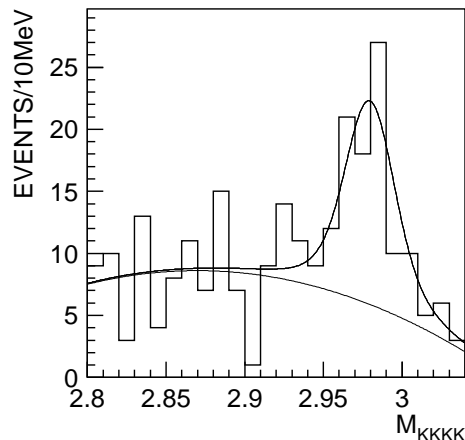


FIG. 10: The  $\eta_c$  fit in the  $M_{\phi\phi}$  distribution.

## B. Results

Fig. 10 shows the  $\eta_c$  fit to the  $M_{\phi\phi}$  distribution. The branching fraction of  $\eta_c \rightarrow \phi\phi$  is determined from

$$\begin{aligned} Br(\eta_c \rightarrow \phi\phi) &= \frac{N^{obs}/\varepsilon}{N_{J/\psi} \cdot Br(J/\psi \rightarrow \gamma\eta_c) \cdot Br^2(\phi \rightarrow K^+K^-)} \\ &= (2.5 \pm 0.5) \times 10^{-3}, \end{aligned}$$

where  $N^{obs} = 76.1$  is the fitted number of  $\eta_c$  events in the  $M_{\phi\phi}$  distribution shown in Fig. 10,  $\varepsilon = 15\%$  is the efficiency determined from Monte Carlo simulation, and  $Br(\phi \rightarrow K^+K^-) = 0.491$  [1]. This result is consistent with the previously published BES result.

## VII. $\eta_c \rightarrow \omega\phi$

$J/\psi \rightarrow \gamma\eta_c \rightarrow \gamma\omega\phi \rightarrow \gamma\pi^+\pi^-\pi^0K^+K^-$  is studied to obtain the  $\eta_c \rightarrow \omega\phi$  branching fraction.

### A. Event Selection

The charged track selection criteria and particle identification are the same as in the  $\eta_c \rightarrow \rho^0\rho^0$  analysis. At least two tracks must be identified as kaons. The photon selection criteria are different for  $\eta_c \rightarrow \omega\phi$  to get higher efficiency because there are three photons in this channel. To reduce the number of spurious low energy photons produced by secondary hadronic interactions, photon candidates must have a minimum energy of 50 MeV and be outside a cone with a half-angle of  $8^\circ$  around any charged track. At least three good photons are required.

To get improved momentum resolution and to remove backgrounds, events are kinematically fitted to the  $J/\psi \rightarrow \gamma\gamma\pi^+\pi^-K^+K^-$  (4C fit) and  $J/\psi \rightarrow \gamma\pi^0\pi^+\pi^-K^+K^-$  (5C fit) hypotheses, using all photons and  $\pi^+\pi^-K^+K^-$  combinations. The combined probability is determined from particle identification probabilities of all tracks and the 4C fit probability to the  $J/\psi \rightarrow \gamma\gamma\pi^+\pi^-K^+K^-$  hypothesis. Candidate events must satisfy  $\chi_{4C}^2(J/\psi \rightarrow \gamma\gamma\pi^+\pi^-K^+K^-) < 25$ ,  $\chi_{5C}^2(J/\psi \rightarrow \gamma\pi^0\pi^+\pi^-K^+K^-) < 20$ ,  $|M_{\pi^+\pi^-\pi^0} - M_\omega| < 0.03 \text{ GeV}/c^2$ , and  $|M_{K^+K^-} - M_\phi| < 0.01 \text{ GeV}/c^2$ .

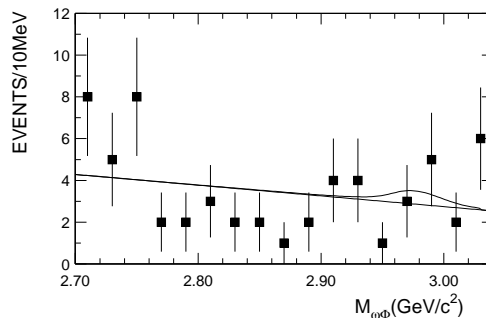


FIG. 11: The  $\eta_c$  fit to the  $M_{\pi^+\pi^-\pi^0 K^+K^-}$  distribution for candidate events.

## B. Results

Figure 11 shows the result of fitting  $\eta_c$  in the  $M_{\pi^+\pi^-\pi^0 K^+K^-}$  distribution of  $J/\psi \rightarrow \gamma\omega\phi$  candidate events. The shape of the  $\eta_c$  used in the fit is obtained from  $\eta_c \rightarrow \omega\phi$  Monte Carlo simulation. The fitted number of  $\eta_c$  events is  $2.1 \pm 6.1$ , which has large errors and includes decays other than  $J/\psi \rightarrow \gamma\omega\phi$  decay. So only an upper limit on  $Br(\eta_c \rightarrow \omega\phi)$  is determined. At the 90% confidence level, the upper limit on  $N_{\eta_c}$  is  $N_{\eta_c}^{upper} = 10$ . The upper limit on  $Br(\eta_c \rightarrow \omega\phi)$  at the 90% C.L. is determined from

$$Br(\eta_c \rightarrow \omega\phi) < \frac{N_{\eta_c}^{upper} / \varepsilon}{N_{J/\psi} \cdot Br(J/\psi \rightarrow \gamma\eta_c) \cdot Br(\phi \rightarrow K^+K^-) \cdot Br(\omega \rightarrow \pi^+\pi^-\pi^0)}$$

$$= 7.1 \times 10^{-4},$$

where  $\varepsilon = 4.2\%$  is the efficiency determined from Monte Carlo.

## VIII. SYSTEMATIC ERRORS

Many sources of systematic errors are considered. Systematic errors associated with efficiencies, such as from MDC tracking, particle identification, photon selection, and kinematic fitting, are determined by comparing  $\psi(2S)$  and  $J/\psi$  data with Monte Carlo simulation for very clean decay channels, such as  $\psi(2S) \rightarrow \pi^+\pi^- J/\psi$ .

The MDC tracking efficiency has been measured using channels like  $J/\psi \rightarrow \Lambda\bar{\Lambda}$  and  $\psi(2S) \rightarrow \pi^+\pi^- J/\psi$ ,  $J/\psi \rightarrow \mu^+\mu^+$ . It is found that the efficiency of the Monte Carlo simulation agrees with that of data within 1-2% per charged track. The total systematic error from the uncertainty of MDC tracking efficiency in our analysis is taken as 8%. The particle identification (PID) efficiency systematic error is calculated by comparing the efficiency of data with that of the Monte Carlo. According to the study of photon detection efficiency in  $J/\psi \rightarrow \rho\pi$  [18], SIMBES simulates the photon detection efficiency in the full energy range within 1 to 3%. Here, 2% is taken as the systematic error in the detection efficiency for each photon.

The systematic errors associated with the kinematic fit are caused by differences between data and simulated data in the momenta and the error matrices of charged tracks and the energies and the directions of neutral tracks. To check the consistency between data and Monte Carlo simulation, two channels,  $J/\psi \rightarrow \rho^0\pi^0$  and  $J/\psi \rightarrow \Lambda\bar{\Lambda}$ , are analyzed for 2-prong and 4-prong events, respectively. The systematic error for 4-prong events caused by the kinematic fit is determined to be 4%. For 4-prong events containing more than one photon, such as  $J/\psi \rightarrow \gamma\eta_c \rightarrow \gamma\omega\omega$  and  $J/\psi \rightarrow \gamma\eta_c \rightarrow \gamma\omega\phi$ , 10% is estimated as the systematic error caused by the kinematic fit.

The choice of different sideband regions can cause differences in  $Br(\eta_c \rightarrow VV)$ . These differences are regarded as the systematic error associated with the choice of sidebands. Changing the fit range, binning, and background shape causes some differences in the result. The largest difference in  $Br(\eta_c \rightarrow VV)$  caused by these changes is taken as the systematic error from these sources.

The  $\eta_c$  mass resolutions used in the fits to determine the number of  $\eta_c$  events are determined from Monte Carlo studies. Differences in  $\eta_c$  mass resolutions between data and Monte Carlo also bring uncertainty to the determination of the branching fraction. The differences in  $Br(\eta_c \rightarrow VV)$  caused by the uncertainty of  $\eta_c$  mass resolution are taken as the systematic error caused by  $\eta_c$  mass resolution.

Many selection requirements are used to remove backgrounds. To estimate the systematic error caused by these, different selection requirements are used. The differences of  $Br(\eta_c \rightarrow VV)$  caused by the change of requirements are taken as systematic errors.

The number of  $J/\psi$  events is  $(57.7 \pm 2.7) \times 10^6$  determined from 4-prong events [10]. The uncertainty of the number of  $J/\psi$  events is 4.7%. The branching fraction of  $J/\psi \rightarrow \gamma\eta_c$  is  $(1.3 \pm 0.4)\%$ , according to the PDG [1]. This will contribute 30% to the systematic error of  $\eta_c \rightarrow VV$ .

TABLE III: Summary of systematic errors for  $\eta_c \rightarrow VV$  (%).

Sources	$\eta_c \rightarrow \rho^0 \rho^0$	$\eta_c \rightarrow K^* \bar{K}^*$	$\eta_c \rightarrow \omega\omega$	$\eta_c \rightarrow \phi\phi$	$\eta_c \rightarrow \omega\phi$
MDC tracking efficiency	8	8	8	8	8
Particle ID	3	3	3	3	3
Detective efficiency of photon kinematic fit	2	2	10	-	6
Different side-bands	4	4	10	4	10
Fit range, binning and background shape	16	12	-	-	-
$\eta_c$ mass resolution	3	7	-	11	-
Different Cuts	7	8	-	7	-
The number of $J/\psi$ events	18	19	14	11	32
$Br(J/\psi \rightarrow \gamma\eta_c)$	4.7	4.7	4.7	4.7	4.7
$Br(J/\psi \rightarrow \gamma\eta_c)$	30	30	30	30	30
Total	40.7	41	37	36	46

Table III lists all systematic error contributions and the total systematic errors. The  $Br(\eta_c \rightarrow VV)$  and  $Br(J/\psi \rightarrow \gamma\eta_c) \cdot Br(\eta_c \rightarrow VV)$  results including systematic errors are listed in Tables IV and V, respectively. Table V results do not have the large systematic error from  $Br(J/\psi \rightarrow \gamma\eta_c)$ .

TABLE IV: Comparison of  $Br(\eta_c \rightarrow VV)$  values between BES and the PDG [1].

Br	BES	PDG
$Br(\eta_c \rightarrow \rho\rho)$	$(1.25 \pm 0.37 \pm 0.51) \times 10^{-2}$	$(2.6 \pm 0.9) \times 10^{-2}$
$Br(\eta_c \rightarrow K^* \bar{K}^*)$	$(10.4 \pm 2.6 \pm 4.3) \times 10^{-3}$	$(8.5 \pm 3.1) \times 10^{-3}$
$Br(\eta_c \rightarrow \omega\omega)$	$< 6.3 \times 10^{-3}$	$< 3.1 \times 10^{-3}$
$Br(\eta_c \rightarrow \phi\phi)$	$(2.5 \pm 0.5 \pm 0.9) \times 10^{-3}$	$(2.6 \pm 0.9) \times 10^{-3}$
$Br(\eta_c \rightarrow \omega\phi)$	$< 1.3 \times 10^{-3}$	-

TABLE V: Summary of  $Br(J/\psi \rightarrow \gamma\eta_c) \cdot Br(\eta_c \rightarrow VV)$ .

Br	BES
$Br(J/\psi \rightarrow \gamma\eta_c) \cdot Br(\eta_c \rightarrow \rho\rho)$	$(1.6 \pm 0.6 \pm 0.4) \times 10^{-4}$
$Br(J/\psi \rightarrow \gamma\eta_c) \cdot Br(\eta_c \rightarrow K^* \bar{K}^*)$	$(1.4 \pm 0.3 \pm 0.5) \times 10^{-4}$
$Br(J/\psi \rightarrow \gamma\eta_c) \cdot Br(\eta_c \rightarrow \omega\omega)$	$< 6.7 \times 10^{-5}$
$Br(J/\psi \rightarrow \gamma\eta_c) \cdot Br(\eta_c \rightarrow \phi\phi)$	$(3.3 \pm 0.6 \pm 0.6) \times 10^{-5}$
$Br(J/\psi \rightarrow \gamma\eta_c) \cdot Br(\eta_c \rightarrow \omega\phi)$	$< 1.4 \times 10^{-5}$

## IX. SUMMARY

The  $Br(\eta_c \rightarrow VV)$  results are compared with PDG values in the Table IV. Table VI compares the ratio of branching fractions with expectations from SU(3) symmetry. The ratios are more consistent with SU(3) symmetry than ratios based on PDG branching fractions, as shown in Table II. Our  $Br(\eta_c \rightarrow \rho\rho)$  result is consistent with the model prediction for  $\Gamma(\eta_c \rightarrow \rho^0 \rho^0)$  of Ref. [3]. The upper limit on  $Br(\eta_c \rightarrow \omega\phi)$  is also given.

## X. ACKNOWLEDGMENT

The BES collaboration thanks the staff of BEPC for their hard efforts. We also thank Prof. Guangda Zhao for helpful discussions. This work is supported in part by the National Natural Science Foundation of China under

TABLE VI: Check of SU(3) symmetry with new BES results. The common systematic error has been removed.

	BR( $10^{-3}$ )	$BR_R(10^{-3})$	Ratio of $BR_R$	SU(3)
$Br(\eta_c \rightarrow \rho\rho)$	$12.5 \pm 4.9$	$6.3 \pm 2.4$	$3.1 \pm 1.2$	3
$Br(\eta_c \rightarrow K^* \bar{K}^*)$	$10.4 \pm 3.2$	$6.1 \pm 1.9$	$3.0 \pm 1.0$	4
$Br(\eta_c \rightarrow \omega\omega)$	$< 6.3$	$< 3.2$	$< 1.6$	1
$Br(\eta_c \rightarrow \phi\phi)$	$2.5 \pm 0.7$	$2.0 \pm 0.6$	$1 \pm 0.3$	1

contracts Nos. 10491300, 10225524, 10225525, 10425523, the Chinese Academy of Sciences under contract No. KJ 95T-03, the 100 Talents Program of CAS under Contract Nos. U-11, U-24, U-25, and the Knowledge Innovation Project of CAS under Contract Nos. U-602, U-34 (IHEP), the National Natural Science Foundation of China under Contract No. 10225522 (Tsinghua University), and the Department of Energy under Contract No. DE-FG02-04ER41291 (U Hawaii).

- 
- [1] S. Eidelman *et al.* (Particle Data Group), Phys. Letts. **B592**, 1 (2004).
  - [2] Y. Jia, G. D. Zhao, High Energy Phys. Nucl. Phys. **23**, 765 (1999) (in Chinese).
  - [3] H. Q. Zhou *et al.*, Phys. Rev. **D71**, 114002 (2005).
  - [4] D. Bisello *et al.*, Nuclear Physics **B350**, 1 (1991).
  - [5] Maurice Benayoun *et al.*, Nuclear Physics **B348**, 327 (1991).
  - [6] J. Z. Bai *et al.* (BES Collaboration), Nucl. Instr. Meth. **A344**, 319 (1994).
  - [7] J. Z. Bai *et al.* (BES Collaboration), Nucl. Instr. Meth. **A458**, 627 (2001).
  - [8] M. Ablikim *et al.* (BES Collaboration), 'The BESII Detector Simulation', to be submitted to Nucl. Instr. and Meth. A.
  - [9] M. Ablikim *et al.* (BES Collaboration), Phys. Rev. **D70**, 112008 (2004).
  - [10] S. S. Fang *et al.*, High Energy Phys. Nucl. Phys. **27**, 277 (2003) (in Chinese).
  - [11] R. M. Baltrusaitis *et al.*, Phys. Rev. **D33**, 1222 (1986).
  - [12] J. Z. Bai *et al.* (BES Collaboration), Phys. Lett. **B472**, 207 (2000).
  - [13] M. Ablikim *et al.* (BES Collaboration), Phys. Lett. **B578**, 16 (2004).
  - [14] M. Chanowitz, Phys. Rev. **D12**, 918 (1975).
  - [15] T. Appelquist *et al.*, Phys. Rev. Lett. **34**, 365 (1975).
  - [16] T. Appelquist *et al.*, Ann. Rev. Nucl. Sci. **28**, 387 (1978).
  - [17] J. C. Chen *et al.*, Phys. Rev. **D62**, 034003 (2000).
  - [18] S.M. Li *et al.*, High Energy Phys. Nucl. Phys. **28**, 64 (2004) (in Chinese).